https://doi.org/10.5194/hess-2022-351
Preprint. Discussion started: 11 October 2022


Hydrology and Earth System Sciences
Discussions

# The most extreme rainfall erosivity ever recorded in China: The "7.20" rainstorm in Henan Province

Yuanyuan Xiao[1], Shuiqing Yin[1], Bofu Yu[2], Conghui Fan[1], Wenting Wang[1], Yun Xie[1]

[1]State Key Laboratory of Earth Surface Processes and Resource Ecology, Faculty of Geographical Science, Beijing Normal University, Beijing, 100875, China
[2]Australian Rivers Institute, School of Engineering and Built Environment, Griffith University, Nathan, Queensland, QLD 4111, Australia

*Correspondence to*: Shuiqing Yin (yinshuiqing@bnu.edu.cn)

**Abstract.** Severe water erosion occurs during extreme storm events. Such an extreme storm occurred in Zhengzhou in central China on 20 July 2021 (the "7.20" rainstorm). The magnitude and frequency of occurrence of this storm event were examined in terms of its erosivity values. To contextualize this extreme event, hourly rainfall data from 2420 automatic meteorological stations in China from 1951 to 2021 were analyzed to: (1) characterize the spatial and temporal distribution of rainfall and rainfall erosivity of the "7.20" rainstorm, (2) evaluate the average recurrence interval of the maximum daily and event rainfall erosivity, and (3) establish the geographical distribution of the maximum daily and event rainfall erosivity in China. The center of the "7.20" rainstorm moved from southeast to northwest in Henan province, and the most intense period of rainfall occurred in the middle and late stages of the storm. Zhengzhou meteorological station happened to be aligned with the center of the storm, with a maximum daily rainfall of 552.5 mm and a maximum hourly rainfall intensity of 201.9 mm·h$^{-1}$. The average recurrence interval of the maximum daily rainfall erosivity (43,354 MJ·mm·ha$^{-1}$·h$^{-1}$) and the maximum event rainfall erosivity (58,874 MJ·mm·ha$^{-1}$·h$^{-1}$) was estimated to be 109,079 and 154,154 years, respectively, assuming the generalized extreme value distribution, and these were the maximum rainfall erosivity ever recorded among 2420 meteorological stations in mainland China. The "7.20" rainstorm suggests that the most erosive of storms does not necessarily occur in the wettest places in southern China, and it can occur in mid-latitude around 35 °N with a moderate mean annual precipitation of 549.2 mm in Zhengzhou meteorological station.

**Keywords.** soil erosion, extreme rainfall, rainfall erosivity, return period

## 1 Introduction

Soil erosion is known as a land degradation process that can affect food production, biodiversity, carbon stocks and ecosystem services (Kebede et al. 2021; Panagos et al., 2015). Soil erosion models are powerful tools to evaluate erosion intensity and the effect of soil and water conservation measures decision makers. The Universal Soil Loss Equation (USLE) (Wischmeier and Smith, 1965, 1978) and its revised USLE (Renard et al., 1997; USDA–ARS, 2013), and the Chinese Soil Loss Equation (CSLE, Liu et al., 2002) are widely used empirical soil erosion models for estimating the long-term average amount of soil loss. Rainfall erosivity quantifies the potential ability of rainfall and runoff to erode the soil and represents the climatic effect on soil erosion as one of the factors in the USLE, RUSLE and CSLE (Yin et al., 2017).

Research has focused on the calculation and estimation of rainfall erosivity, and its spatial and temporal variations (Yin et al., 2017). High temporal resolution data are often used to estimate the rainfall erosivity ranging between 1-min and 60-min intervals in most studies (Klik et al., 2015; Lu and Yu, 2002; Ma et al., 2014; Panagos et al., 2015, 2016; Xie et al., 2016; Yin et al., 2015;). As rainfall data with high temporal resolution in most parts of the world are limited in terms of the record length and spatial coverage, it is often necessary to establish simple relationships between rainfall erosivity values based on data with finer and coarser resolutions, and then apply these relationships to regions with data in coarser resolution only (Xie et al., 2016;

Yin et al., 2015; Zhu and Yu, 2015). Since soil erosion is difficult to measure at large scales, soil erosion models are often used for estimating soil loss by water erosion at regional, national and global scales. Rainfall erosivity maps can provide rainfall erosivity values with rainfall observations and without observations and the generation of erosivity maps is one of necessary procedures for estimation of soil loss using most empirical soil erosion models (Bezak et al. 2021, 2022; McGehee et al., 2022; Yue et al., 2022). Rainfall erosivity maps were usually generated by the interpolation of rainfall erosivity values from at-site rainfall observations by geostatistics techniques, such as the inverse distance weighting, ordinal Kriging and so on (Panagos et al., 2015; Sadeghi et al., 2017; Yin et al., 2019). Available gridded rainfall data, such as satellite precipitation products and climate reanalysis data can also be used to generate rainfall erosivity maps (Panagos et al., 2017; McGehee et al., 2022; Yue et al., 2022). Auerswald et al. (2019) used 1 km resolution radar rainfall data to produce the average rainfall erosivity maps with 1 km in resolution in Germany from 2001 to 2017. Temporal variations in rainfall erosivity are important for understanding changes in soil erosion and assessing the future climate change impact on the land degradation. At present, research on the temporal change of rainfall erosivity mainly focuses on past changes (Cao et al., 2018; Qin et al.2016; Wang et al., 2022; Yang, 2015; Zhang et al, 2010) and future projections (Kilic et al 2021; Panagos et al., 2022).

Most studies have focused on the long-term average of rainfall and rainfall erosivity characteristics (Gu et al., 2020; Li et al., 2008; Liu et al. 2019; Yin et al., 2019), and have assessed the intensity and frequency of extreme rainfall events at the regional, national and global levels (Alexander et al., 2007; Almagro et al., 2017; Evans et al., 2016; Nearing et al., 2004). However, there are few studies of rainfall erosivity of extreme events (Diodato et al., 2016; Wang et al., 2022). The long-term average value cannot fully reflect the severity of soil erosion process, and a few severe soil erosion events can contribute a great deal to the total amount of soil lost over many years (Bezak et al. 2021; Borrelli et al., 2016; Meusburger et al., 2012; Petek et al., 2018). For example, field observations at the plot scale in eastern Austria showed that the three largest erosion events from 1994 to 2019 accounted for 79% of the total soil loss over the same period (Klik and Rosner, 2020). Zhou et al. (1992) reported that high-intensity, short-duration heavy precipitation events accounted for about 90% of the total annual soil erosion in the Loess Plateau.

Extreme rainfall, which varies a great deal in space and time, can lead to severe flooding, with far-reaching implications for socio-economic and human activities (Fishman, 2016). With global warming, the frequency and intensity of extreme precipitation events are increasing in most mid-latitudes (Fang et al., 2017; IPCC 2021; Liao et al., 2019; Liu et al., 2017). Extreme rainfall, especially rainfall events with high intensity, is often more erosive (Fang et al., 2018; Huang et al., 2016a, 2016b, 2016c). Many studies reported that satellite-based products tend to underestimate the extreme rainfall, which can have an important effect on the estimation of rainfall erosivity based on satellite-based products (Jiang et al., 2019; Palharini et al., 2020; Rahmawati and Lubczynski., 2018). For example, Bezak et al. (2022) showed CMORPH estimates had a marked tendency to underestimate rainfall erosivity of high erosive areas when compared to the GloREDa estimates. In addition, underestimation of extreme rainfall from climate models will cause conservative projections of erosivity in high erosive areas in the future (Panagos et al., 2022). Therefore, it is of great interest to examine the magnitude and frequency of occurrence of rainfall and rainfall erosivity of extreme storm events.

An extraordinarily heavy rainfall event occurred between 17 and 22 of July 2021 in Henan Province. Such a rare event was never experienced or recorded in recent times in China. Record daily rainfall was observed at 10 national meteorological observation stations in Zhengzhou, Xinxiang, Kaifeng, Zhoukou, Luoyang and other cities in Henan Province. Zhang et al. (2021) reported the storm was influenced by several weather systems including the eastward extension of the South Asian high, the abnormal northerly subtropical high, the Bengal Bay Depression at low latitude, the typhoon Cempaka in the South China Sea and the typhoon in the Western Pacific. The strengthen and eastward extension of the South Asia high leads to an obvious divergence area of the upper atmosphere over Henan Province, which is conducive to the upward movement of the lower atmosphere. The subtropical high, which is stronger and northward moving than the same period in normal years, the No. 6

https://doi.org/10.5194/hess-2022-351
Preprint. Discussion started: 11 October 2022




typhoon “Fireworks” and the No. 7 typhoon “Chapaca” in low latitudes, and the low pressure in Bengal Bay have led to the stable and lasting transmission of warm and humid air flow to Henan Province. Taihang Mountain and Funiu Mountain in the northwestern and western Henan Province blocked the air flow, and a strong convergence formed in front of mountains, resulting in this extreme rainfall event.

The maximum hourly rainfall between 16:00 and 17:00 on 20 July reached 201.9 mm at Zhengzhou meteorological station, the highest ever recorded in China (Zhang et al., 2021). It has been widely reported that this extreme storm caused extensive flooding and landslides with damages to infrastructure and loss of human lives (Jin et al., 2022; Zhang et al., 2022). Event total rainfall, daily and hourly rainfall of the “7.20” rainstorm have been reported elsewhere (Zhang et al. 2021), but rainfall erosivity associated with this extreme storm is still unknown. The “7.20” rainstorm presents a rare opportunity to examine the extreme rainfall erosivity in China. Thus, hourly rainfall data were used to evaluate the maximum daily and event rainfall erosivity, to estimate its average recurrence interval, to contextualize geographically the extreme erosivity of the “7.20” rainstorm, to demonstrate how extreme the erosivity value of the “7.20” rainstorm was and how large event rainfall erosivity could be in China, and to highlight the need to pay attention to extreme storms and the huge erosion risk associated with them in the future.

## 2 Material and Methods

### 2.1 Data source and pre-processing

Observed hourly rainfall data from 1951 to 2021 for 2420 meteorological stations in China were acquired from China Meteorological Administration (CMA) and the data had been quality-controlled by CMA’s National Meteorological Information Center. Hourly rainfall data from 797 meteorological stations in Henan and its surrounding nine provinces (municipalities) from 20:00 (Beijing time) on 16 July and to 20:00 on 22 July 2021 were used to characterize the “7.20” rainstorm. Hourly rainfall data from 1951 to 2020 were as historical data. In order to reduce the impact of missing values on the result, years with missing data were discarded. A year with missing data was defined as follows: if there were 4 or more hours of missing records on a given day, it was considered as a missing day and if the number of missing days in a month ≥ 6, it was considered as a missing month. Since most of the rainfall in the north of China (north of 32°N) is concentrated from May to September, the year with any month from May to September missing was defined as a missing year. In the south of China, the year with any month from April to October missing is defined as a missing year. Missing values in effective years are input as 0.

https://doi.org/10.5194/hess-2022-351
Preprint. Discussion started: 11 October 2022

Hydrology and Earth System Sciences
Discussions

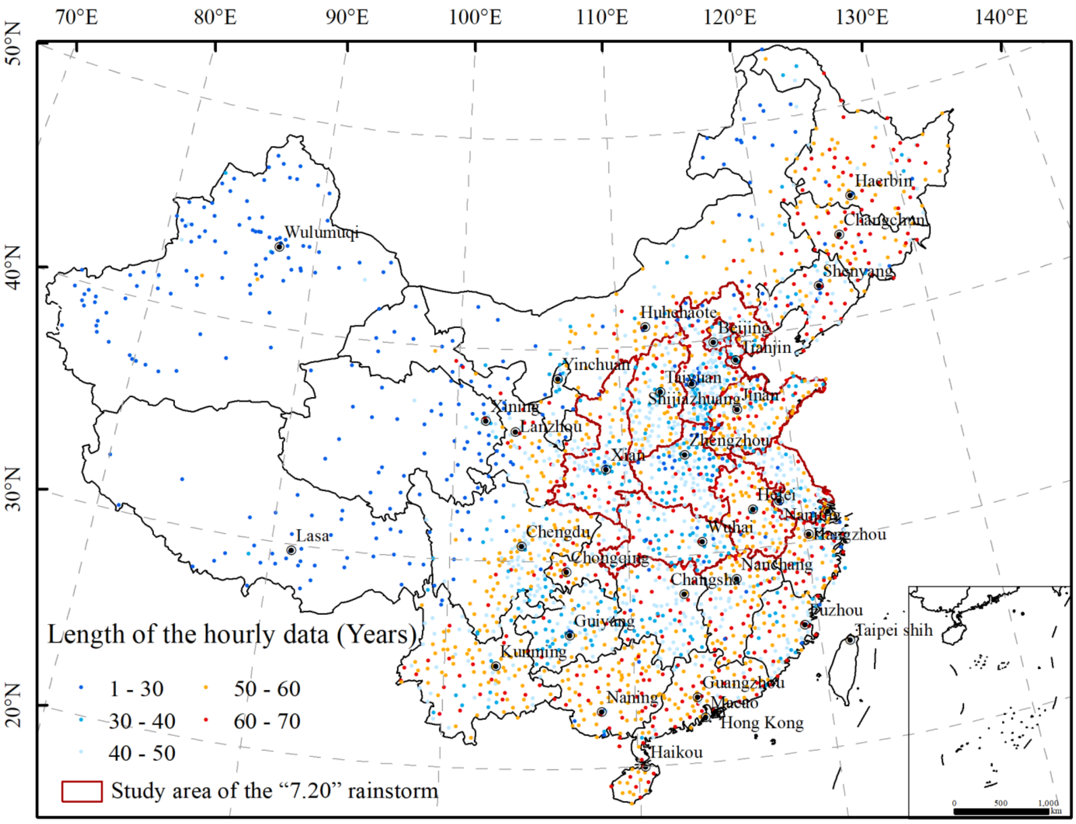


**Figure 1.** Spatial distribution of stations with hourly rainfall data and the record length.

## 2.2 Framework of study

### *2.2.1 Definition of rainfall events and rainfall parameters*

An event was defined as the duration of rainfall with dry periods less than "minimum inter-event time" (MIT). The MIT in the USLE and RUSLE2 was 6 h. In this study, the storm was divided into events when the time of no rainfall was over 6 hours. The maximum event rainfall, maximum daily rainfall, maximum hourly rainfall and maximum event rainfall erosivity were computed following to the framework of Fig. 2. There were several erosive events over the 6-day period during the "7.20" rainstorm. The maximum event rainfall was associated with the erosive event with the maximum rainfall amount, and it was not the total rainfall amount over the 6 days. Maximum event rainfall erosivity was similarly defined.

### *2.2.2 Calculation of the energy and daily/event rainfall erosivity*

Erosive events were used to calculate the daily and event rainfall erosivity, $EI_{30}$ (MJ·mm·ha$^{-1}$·h$^{-1}$), which is the product of the event energy and peak 30-min intensity.

Rainfall kinetic energy is a function of raindrop size and falling velocity. The total energy ($E$, MJ·ha$^{-1}$) of an erosive event was estimated using the following equations (USDA-ARS, 2013):

$$e_r = 0.29 \cdot [1 - 0.72 \cdot exp(-0.082 \cdot i_r)] \quad (1)$$

$$E = \sum_{r=1}^{l}(e_r \cdot P_r) \quad (2)$$

where a rainfall event was divided into $l$ periods with a constant intensity, $i_r$ (mm·h$^{-1}$) for the $r^{th}$ period, $P_r$ (mm) was the rainfall amount for the $r^{th}$ period and $e_r$ ($MJ \cdot ha^{-1} \cdot mm^{-1}$) was the unit energy per unit rainfall ($MJ \cdot mm^{-1} \cdot ha^{-1}$) for the $r^{th}$ period. The event rainfall erosivity can be estimated with of $E$ and $I_{1h}$:

$$EI_{1h} = E \cdot I_{1h} \tag{3}$$

$$EI_{30} = 1.489 \cdot EI_{1h} \tag{4}$$

where $I_{1h}$ was the peak 1-hour rainfall intensity for the erosive event, and the conversion factor of 1.489 was used to correct the bias of estimated rainfall erosivity using hourly rainfall data (Yue et al., 2020).

Total rainfall and energy over the 6 days of the "7.20" rainstorm for 797 stations were interpolated into grid data with 100 m spatial resolution, and regional averages of Henan province and the study area (Henan province and its surrounding nine provinces/municipalities) were calculated and compared with Zhengzhou meteorological station.

*2.2.3 Generalized extreme value distribution model and parameter estimation*

An annual series is defined here as a collection of maxima, one from each calendar year. Annual series of the maximum daily and event rainfall erosivity from 1951-2020 ($n$ = 67 due to three missing years) for Zhengzhou meteorological station were sorted in a descending order with the largest assigned a rank of 1. The empirical return period, or the average recurrence interval, of each observation in the annual series was calculated according to the following formula:

$$RP = \frac{n+1}{m} \tag{5}$$

where $RP$ is the empirical return period in years, $n$ the number of years or the sample size, and $m$ the rank ($m$ = 1 for the largest).

The annual series of the maximum daily rainfall erosivity and the annual maximum event rainfall erosivity from 1951-2020 for Zhengzhou meteorological station were used to fit the Generalized Extreme Value (GEV) distribution, respectively. The probability distribution function of GEV can be expressed (Li et al., 1988; Huang et al., 2020) as:

$$F(x) = e^{-(1+k\frac{x-\mu}{\sigma})^{-\frac{1}{k}}} \tag{6}$$

where $k$ was the shape parameter, $\sigma$ the scale parameter and $\mu$ the position parameter. The estimated value of rainfall erosivity with a return period $T$ is $X_T$ as follows:

$$X_T = \begin{cases} \mu + \frac{\sigma}{k}\left\{1 - \left[-log(1-\frac{1}{T})\right]^{-k}\right\} & k \neq 0 \\ \mu + \sigma\left\{1 - \left[-log(1-\frac{1}{T})\right]\right\} & k = 0 \end{cases} \tag{7}$$

where log is natural log. Method of L-moments was used for the parameter estimation (Hosking, 1990). L-moments is a linear combination of probability weighted moments (PWMs), and the estimated value has good robustness. Among them, the $r^{th}$ order probability weighted moment of random variable $x$ is:

$$B_r = E[x \cdot F(x)^r] \tag{8}$$

By sorting sample of size $n$ from the smallest to the largest, the following estimates can be obtained:

$$\widehat{b_0} = \frac{1}{n}\sum_{j=1}^{n} x_j \tag{9}$$

$$\widehat{b_1} = \frac{1}{n}\sum_{j=1}^{n-1} \frac{(n-j)}{(n-1)} x_j \tag{10}$$

$$\widehat{b_2} = \frac{1}{n}\sum_{j=1}^{n-2} \frac{(n-j)(n-j-1)}{(n-1)(n-2)} x_j \tag{11}$$

$$\widehat{b_3} = \frac{1}{n}\sum_{j=1}^{n-3} \frac{(n-j)(n-j-1)(n-j-2)}{(n-1)(n-2)(n-3)} x_j \tag{12}$$

L-moments can be obtained by a linear combination of the above estimates:

$$l_1 = \widehat{b_0} \tag{13}$$

$$l_2 = 2 \cdot \widehat{b_1} - \widehat{b_0} \tag{14}$$

$$l_3 = 6 \cdot \widehat{b_2} - 6 \cdot \widehat{b_1} + \widehat{b_0} \tag{15}$$

https://doi.org/10.5194/hess-2022-351
Preprint. Discussion started: 11 October 2022



$$l_4 = 20 \cdot \widehat{b_3} - 30 \cdot \widehat{b_2} + 12 \cdot \widehat{b_1} - \widehat{b_0} \quad (16)$$

where $\tau_3$ is l-skewness, $\tau_4$ is l-kurtosis, which can be calculated with the ratio of L-moments:

$$\tau_3 = \frac{l_3}{l_2}, \quad \tau_4 = \frac{l_4}{l_2} \quad (17)$$

From the set of equations above, parameters of the GEV distribution can be estimated:

$$\hat{z} = \frac{2}{3+\tau_3} - \frac{ln2}{ln3} \quad (18)$$

$$\hat{k} \approx 7.859 \cdot \hat{z} + 2.9554 \cdot \hat{z}^2 \quad (19)$$

$$\hat{\sigma} = \frac{l_2 \cdot \hat{k}}{(1-2^{-\hat{k}}) \cdot \Gamma(1+\hat{k})} \quad (20)$$

$$\hat{\mu} = l_1 + \hat{\sigma}\frac{\Gamma(1+\hat{k})-1}{\hat{k}} \quad (21)$$

where $\Gamma(\cdot)$ is the gamma function.

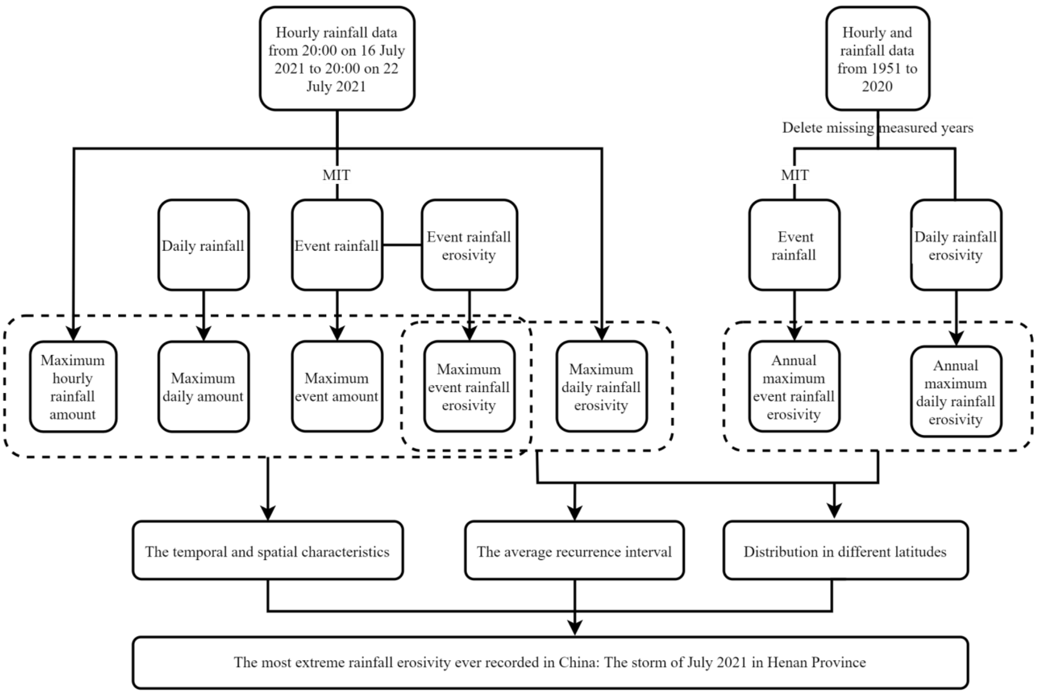


**Figure 2.** Study framework

## 3 Results and discussion

### 3.1 Temporal and spatial characteristics of the "7.20" rainstorm

#### *3.1.1 Characteristics of the "7.20" rainstorm*

The extreme event occurred in Henan Province between 20:00 on 16 July 2021 and 20:00 on 22 July 2021. The center of the storm center is mainly located around Zhengzhou. The storm duration was long and accumulated rainfall was huge. Spatial pattern of accumulated rainfall from 20:00 on 16 July 2021 to 20:00 on 22 July 2021 is shown in Fig. 3a. The top three rainfall stations were Zhengzhou (817.3 mm), Huixian (755.2 mm) and Xinmi (723.5 mm). Additionally, among the 797 automatic

https://doi.org/10.5194/hess-2022-351
Preprint. Discussion started: 11 October 2022

Hydrology and Earth System Sciences
Discussions
Open Access

meteorological stations in the study area, 58 meteorological stations have accumulated rainfall of more than 250 mm, of which 50 are located in Henan Province. Rainfall mass curves for these three stations are shown in Fig. 3b. Obviously, the rainstorm at Zhengzhou meteorological station and Xinmi station contributed more than 50 % of the rainfall in the middle period, while the rainstorm at Huixian station contributed more than 50 % of the rainfall in the last period. Wang et al. (2016) has demonstrated that different rainstorm patterns with rainfall peak in the early, middle and late stages have different effects on soil erosion process, under the natural rainfall conditions. It showed that given the same $EI_{30}$, the rainstorm pattern with rainfall peak at the later stage produced more soil loss than the other patterns.

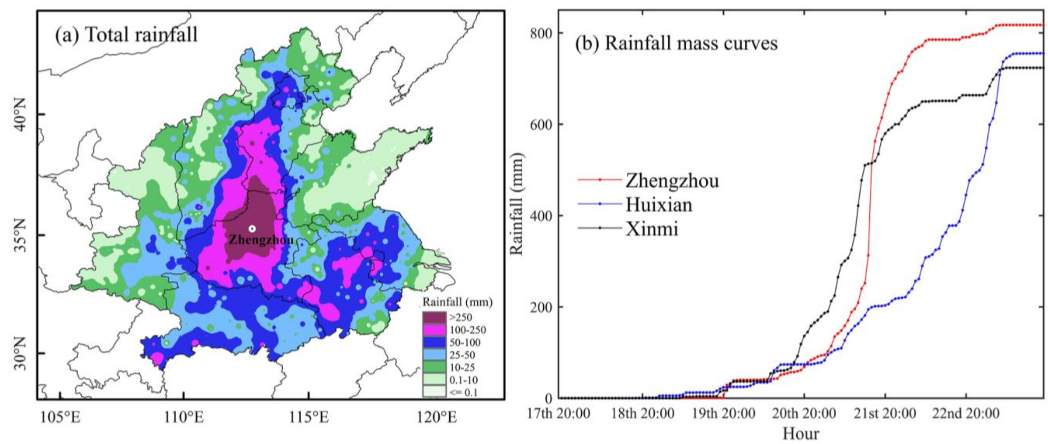


**Figure 3.** Total rainfall over the study area from 20:00 on 16 July 2021 to 20:00 on 22 July 2021, and rainfall mass curves for 3 stations with the largest rainfall totals.

Spatial pattern of daily rainfall in study area from 20:00 on 16 July 2021 to 20:00 on 22 July 2021 is shown in Fig. 4. Heavy rainfall mainly occured in the middle and late stages of the event. The maximum daily rainfall (Zhengzhou, 552.5 mm) occurred on 20 July (Fig. 4d), while the storm was most extensive on 21 July (Fig. 4e). The storm is initially concentrated in the southeast of Henan and Anhui Provinces (Fig. 4a), and then dispersed somewhat on 18 July (Fig. 4b). On 19 July , the storm re-appears in the central region of Henan Province (Fig. 4c). On 20 July, the storm began to intensify and expand its spatial extent (Fig. 4d). The daily rainfall at 39 meteorological stations exceeded 100 mm, and the daily rainfall of 7 meteorological stations exceeded 250 mm on 20 July. On 21 July (Fig. 4e), the center of the storm began to move northward, and the rainfall intensity started to dissipate, and the storm now covered a large area with storm center drifted north to Tangyin (388.2 mm), Henan Province, and recorded rainfall at 48 meteorological stations exceeded 100 mm and 6 meteorological stations exceeded 250 mm. The rainfall decreased considerably by 22 July (Fig. 4f). The storm center was located in the north of Henan Province, and the rainfall at 16 meteorological stations exceeded 100 mm.

https://doi.org/10.5194/hess-2022-351
Preprint. Discussion started: 11 October 2022


Hydrology and Earth System Sciences
Discussions

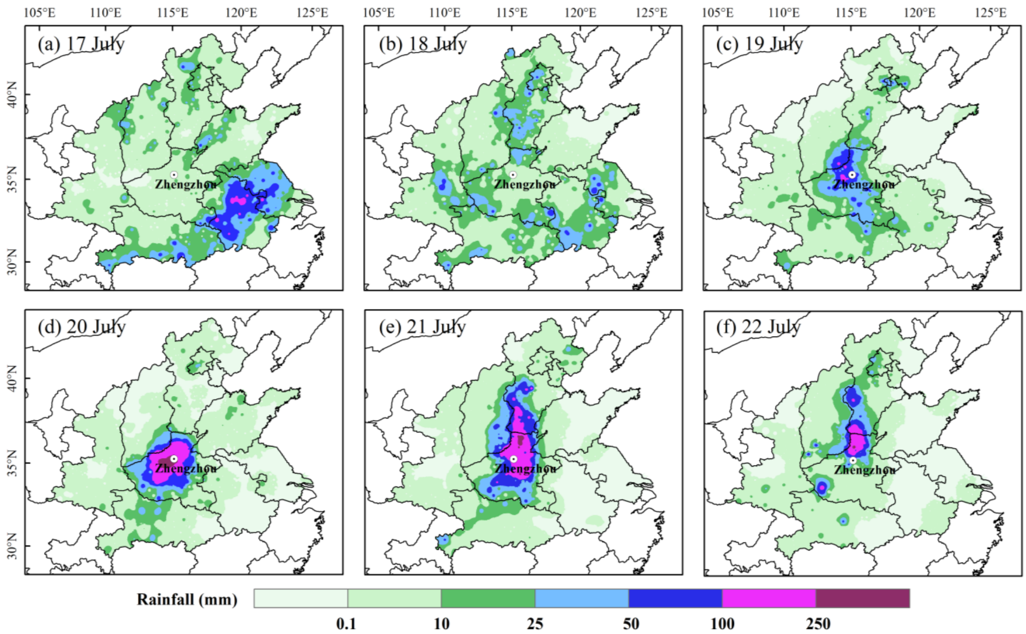


**Figure 4.** Spatial pattern of daily rainfall in the study area. Daily rainfall is rainfall accumulation over 24-hour period, e.g. daily rainfall on 20 July is the total rainfall from 20:00 on 19 July to 20:00 on 20 July.

### *3.1.2 The spatial distribution of rainfall parameters and rainfall erosivity*

The spatial distribution of maximum daily and hourly rainfall amount, and maximum event rainfall and rainfall erosivity are shown in Fig. 5. At the center of the storm, a maximum event rainfall amount of 785.1 mm and a maximum daily rainfall amount of 552.5 mm on 20 July were recorded at Zhengzhou meteorological station. From 16:00 to 17:00 on 20 July, maximum hourly rainfall reached 201.9 mm at Zhengzhou meteorological station, and created a new hourly rainfall intensity record in mainland China. The maximum event rainfall erosivity in the area with Zhengzhou meteorological station has reached 58874 $MJ \cdot mm \cdot ha^{-1} \cdot h^{-1}$.

https://doi.org/10.5194/hess-2022-351
Preprint. Discussion started: 11 October 2022


Hydrology and Earth System Sciences
Open Access
Discussions

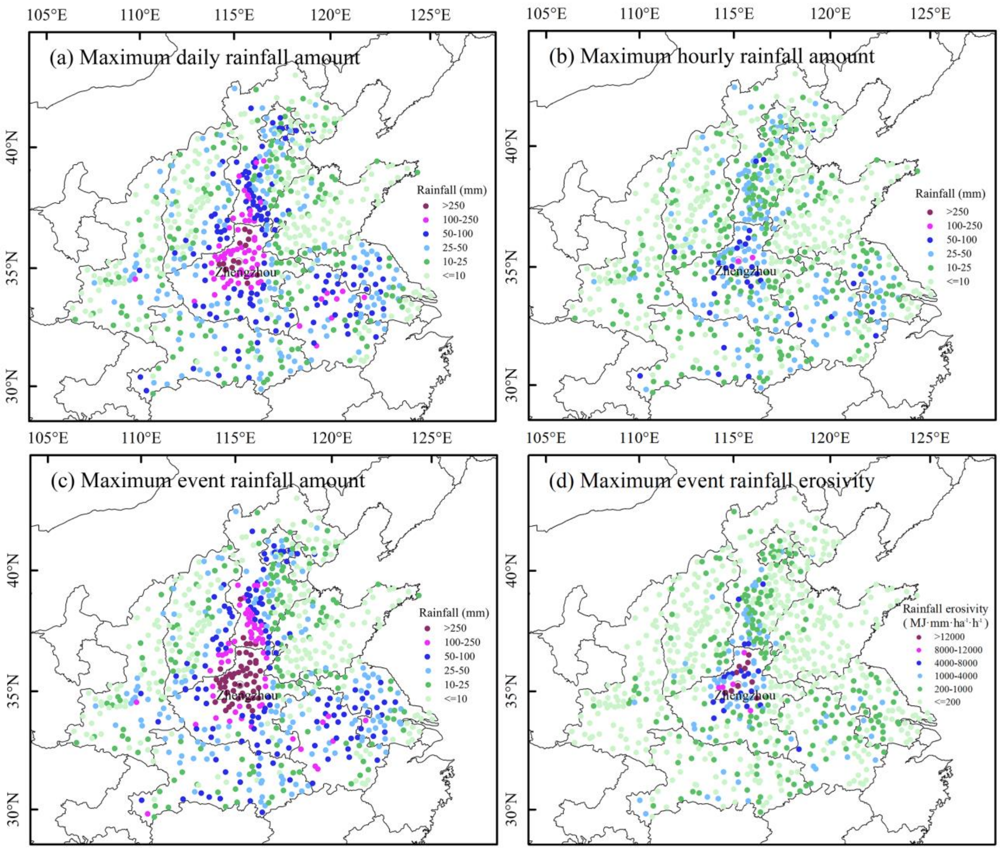


**Figure 5.** Spatial distribution of rainfall amount and rainfall erosivity associated with the "7.20" rainstorm.

### *3.1.3 Rainfall's total kinetic energy*

**Table 1.** The composition of average rainfall and energy in different regions from 20:00 on 16 July 2021 to 20:00 on 22 July 2021

| Region | Index | 17th | 18th | 19th | 20th | 21st | 22nd | Total |
|---|---|---|---|---|---|---|---|---|
| Study area ($1.33\times10^8$ ha) | Mean rainfall (mm) | 12.4 | 10.0 | 6.8 | 8.7 | 11.3 | 5.8 | 55.0 |
| | E ($MJ\cdot ha^{-1}$) | 2.6 | 2.0 | 1.3 | 1.7 | 2.3 | 1.1 | 11.0 |
| Henan province ($1.66\times10^7$ ha) | Average rainfall (mm) | 5.8 | 13.5 | 26.6 | 70.5 | 61.9 | 21.5 | 199.8 |
| | E ($MJ\cdot ha^{-1}$) | 2.0 | 3.0 | 4.8 | 13.5 | 15.6 | 7.1 | 46.0 |
| Zhengzhou meteorological station | Average rainfall (mm) | 0.0 | 1.3 | 60.2 | 552.5 | 176.0 | 27.3 | 817.3 |
| | E ($MJ\cdot ha^{-1}$) | 0.0 | 0.1 | 12.3 | 144.2 | 40.0 | 4.0 | 200.6 |

The detachment of soil particles from the soil mass and the transportation of detached particles by raindrop impact and surface water flow are two main processes of soil erosion. Rainfall energy reflects the impact of raindrop detachment on the soil. The average rainfall and energy for each meteorological day over different regions from 20:00 on 16 July 2021 to 20:00 on 22 July 2021 were listed in Table. 1. Comparing the three regions, the average rainfall and E in the study area on 17 July are higher than those in Henan Province and Zhengzhou meteorological station, indicating that the rainstorm center may be outside Henan Province at this time. With the movement of rainstorm center, the average rainfall and E of Henan Province and Zhengzhou meteorological station gradually increase. The average rainfall in Henan Province reached its peak on 20 July (70.5

https://doi.org/10.5194/hess-2022-351
Preprint. Discussion started: 11 October 2022



mm), but E reached its peak on 21 July (15.6 MJ·ha$^{-1}$). The average rainfall and E of Zhengzhou meteorological station reached the peak on 20 July, which were 552.5 mm and 144.2 MJ·ha$^{-1}$ respectively. The energy of Zhengzhou meteorological station on 20 July is 11 times of average energy in Henan Province. Land vegetation, including forests, shrubs and grass, provide the important protection from the direct detachment of raindrops.

### 3.2 How extreme is the event recorded at Zhengzhou meteorological station?

*3.2.1 Frequency of occurrence the maximum daily and event rainfall erosivity*

Annual maximum daily rainfall erosivity and the annual maximum event rainfall erosivity in Zhengzhou meteorological station from 1951 to 2020 are shown in Fig. 6 along with fitted GEV distribution. It can be seen from Fig. 6 that the GEV distribution fits the maximum daily rainfall erosivity and the maximum event rainfall erosivity well. Using the fitted GEV distribution, the average recurrence interval of the maximum daily rainfall erosivity of the "7.20" rainstorm is estimated to be about 1 in 109,079 years, and the ratio of the observed daily erosivity (43354 MJ·mm·ha$^{-1}$·h$^{-1}$) over 1-in-100-year daily erosivity (4798 MJ·mm·ha$^{-1}$·h$^{-1}$) is 9.04. Similarly, the average recurrence interval of the maximum event rainfall erosivity is estimated to be about 1 in 154,154 years, the observed event erosivity of the “7.20” rainstorm (58,874 MJ·mm·ha$^{-1}$·h$^{-1}$) is 9.45 times larger than the 1-in-100-year event erosivity (6229 MJ·mm·ha$^{-1}$·h$^{-1}$). Evidently, compared with observations in the past decades (1951-2020), the maximum daily and event rainfall erosivity of the "7.20" rainstorm in 2021 is extraordinary, and the event is so rare and extreme that it should be regarded as an outlier among observations in other years.

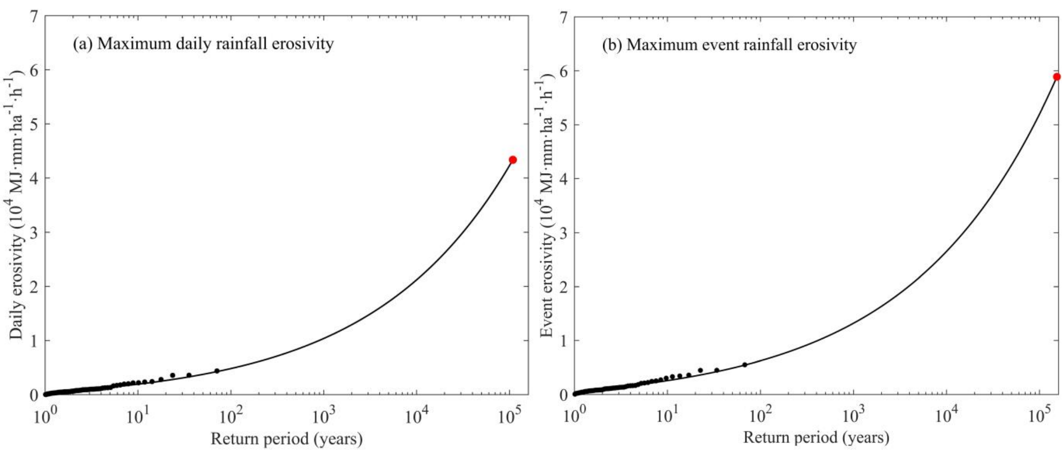


**Figure 6.** Observed daily (a) and event (b) rainfall erosivity as a function of the empirical and return period at Zhengzhou meteorological station (black solid circles are observations from the period 1951-2020, the red solid circles indicate the “7.20” rainstorm in 2021, and the solid lines in black represent the fitted GEV distribution using observations from 1951-2020)

*3.2.2 Distribution of the maximum rainfall erosivity in different latitudes*

Geographical distribution of the maximum daily rainfall erosivity ever recorded at each of 2420 meteorological stations in China is shown as a function of the latitude in Fig. 7. Envelope curves I and II are drawn for the scatter plot, and the stations and the corresponding daily rainfall and rainfall erosivity values that were used to define these envelope curves are given in Table. 2. The two envelope curves overlap at three stations at low latitude and one at high latitude, and the change from curve I to II in the middle latitude is entirely a result of the “7.20” rainstorm in 2021. Prior to the “7.20” rainstorm, curve I shows that the maximum recorded daily rainfall erosivity decreases from about 20°N as the latitude increases, and the maximum daily erosivity value was 39345 MJ·mm·ha$^{-1}$·h$^{-1}$, recorded Maoming meteorological station in Guangdong Province (21.75°N)

https://doi.org/10.5194/hess-2022-351
Preprint. Discussion started: 11 October 2022

Hydrology and Earth System Sciences
Open Access
Discussions

on 5 June 2020. Post the "7.20" rainstorm, the maximum daily rainfall erosivity ever recorded was increased to 43354 MJ·mm·ha$^{-1}$·h$^{-1}$ or by more than 10 % at Zhengzhou meteorological station (34.72°N) on 20 July 2021.

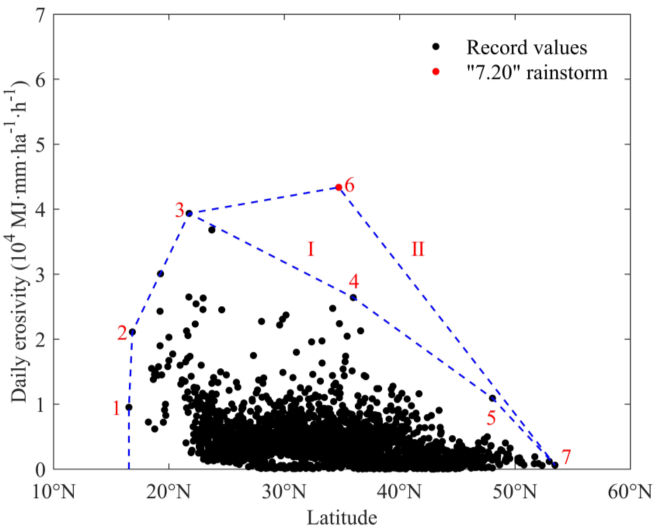


**Figure 7.** The maximum recorded daily rainfall erosivity as a function of latitude for China. The point enclosed by the envelope curve I is the maximum daily rainfall erosivity of each station from 1951 to 2020. The point enclosed by envelope curve II is the maximum daily rainfall erosivity of each station from 1951 to 2021.

**Table 2.** The mean annual rainfall, maximum daily rainfall and rainfall erosivity for stations to define envelope curves.

| ID | | Station ID | Station name | Latitude | Mean annual rainfall (mm) | Daily rainfall (mm) | Daily rainfall erosivity (MJ·mm·ha$^{-1}$·h$^{-1}$) | Date |
|---|---|---|---|---|---|---|---|---|
| I | II | | | | | | | |
| 1 | 1 | 59985 | Shanhu | 16.53 | 1316.0 | 227.6 | 9512 | 1980-09-12 |
| 2 | 2 | 59981 | Xisha | 16.83 | 1467.9 | 585.6 | 21104 | 1995-09-05 |
| 3 | 3 | 59659 | Maoming | 21.75 | 1701.7 | 307.3 | 39345 | 2020-06-05 |
| 4 | | 54848 | Zhucheng | 35.98 | 623.8 | 592 | 26398 | 1999-08-12 |
| 5 | | 50658 | Keshan | 48.05 | 445.4 | 179.6 | 10909 | 1957-07-15 |
| | 6 | 57083 | Zhengzhou | 34.72 | 566.7 | 552.5 | 43354 | 2021-07-20 |
| 7 | 7 | 50137 | Beijicun | 53.47 | 385.2 | 77.6 | 603 | 2010-07-31 |

Geographical distribution of the maximum event rainfall erosivity ever recorded at each of 2420 meteorological stations in China is shown as a function of the latitude in Fig. 8. Envelope curves I and II are drawn for the scatter plot, and the stations and the corresponding event rainfall and rainfall erosivity values that were used to define these envelope curves are given in Table. 3. The two envelope curves overlap at three stations at low latitude and one at high latitude, and the change from curve I to II in the middle latitude is entirely a result of the extreme "7.20" rainstorm in 2021. Prior to the "7.20" rainstorm, curve I shows that the maximum recorded event rainfall erosivity decreases from about 20°N as the latitude increases, and the maximum ever event erosivity value was 41537 MJ·mm·ha$^{-1}$·h$^{-1}$, recorded Maoming meteorological station in Guangdong Province (21.75°N) from 20:00 on 20 May 1987 to 18:00 on 22 May 1987. Post the "7.20" rainstorm, the maximum event rainfall erosivity ever recorded was increased to 58874 MJ·mm·ha$^{-1}$·h$^{-1}$, or an increase of more than 40 % at Zhengzhou meteorological station (34.72°N) on 20 July 2021.

https://doi.org/10.5194/hess-2022-351
Preprint. Discussion started: 11 October 2022

Hydrology and Earth System Sciences
Open Access
Discussions

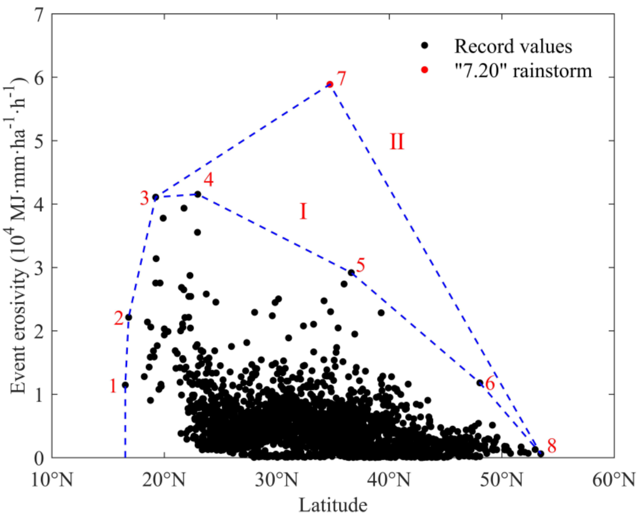


**Figure 8.** The maximum recorded event rainfall erosivity as a function of latitude for China. The point enclosed by the envelope curve I is the maximum event rainfall erosivity of each station from 1951 to 2020. The point enclosed by envelope curve II is the maximum event rainfall erosivity of each station from 1951 to 2021.

**Table 3.** The mean annual rainfall, maximum event rainfall and rainfall erosivity for stations to define envelope curves.

| ID | | Station ID | Station name | Latitude | Starting date and time | End date and time | Mean annual rainfall (mm) | Event rainfall (mm) | Event rainfall erosivity (MJ·mm·ha$^{-1}$·h$^{-1}$) |
|---|---|---|---|---|---|---|---|---|---|
| I | II | | | | | | | | |
| 1 | 1 | 59985 | Shanhu | 16.53 | 1980-09-11 11:00 | 1980-09-12 8:00 | 1316.0 | 288.2 | 11446 |
| 2 | 2 | 59981 | Xisha | 16.83 | 1995-09-05 8:00 | 1995-09-06 23:00 | 1467.9 | 625.5 | 22135 |
| 3 | 3 | 59855 | Qionghai | 19.23 | 2010-10-01 22:00 | 2010-10-08 15:00 | 2021.7 | 1433.3 | 41083 |
| 4 | | 59500 | Haifeng | 22.97 | 1987-05-20 20:00 | 1987-05-22 18:00 | 2407.5 | 987.3 | 41537 |
| 5 | | 53892 | Handan | 36.62 | 1963-08-03 3:00 | 1963-08-06 1:00 | 478.8 | 748.1 | 29174 |
| 6 | | 50658 | Keshan | 48.05 | 1957-07-15 14:00 | 1957-07-15 24:00 | 445.4 | 199.5 | 11794 |
| | 7 | 57083 | Zheng-zhou | 34.72 | 2021-07-18 8:00 | 2021-07-21 10:00 | 566.7 | 785.1 | 58874 |
| 8 | 8 | 50137 | Beijicun | 53.47 | 2010-07-30 23:00 | 2010-07-31 14:00 | 385.2 | 77.6 | 603 |

A large number of studies have shown that the mean annual rainfall and rainfall erosivity, i.e. the R-factor, decrease from southeast to northwest in China (Yin et al., 2019; Yue et al., 2022), that is, the mean annual rainfall and rainfall erosivity are the highest at low latitude in China. Like rainfall, the average rainfall intensity for given storm duration also tends to be high at low latitude, and low at high latitude in China (Bureau of Hydrology et al., 2001). Thus, one would expect that maximum daily and event rainfall erosivity tends to decrease with latitude, a trend largely supported by the envelope curve I in Fig. 7 & 8. The "7.20" rainstorm may have fundamentally changed the nature and distribution of extreme daily and event erosivity in China as we knew them up to now. This is consistent with the research of Wang et al. (2002), and the rainstorm extreme value does not always conform to the pattern of decreasing from low latitude to high latitude. For example, based on measured and surveyed rainfall records, the maximum 24-hour rainfall depth occurred at Linzhuang meteorological Station in Henan Province in the mid-latitude on 7 August 1975 (Wang et al., 2002). Occurrence of this "7.20" rainstorm in 2021 around Zhengzhou has important implications. First, Figure. 7 & 8 suggest that extreme event erosivity may be the highest in mid-

Hydrology and Earth System Sciences
Discussions

latitude around 35°N despite the fact the mean annual rainfall and rainfall intensity are by no means the highest in mid-latitude in China. Second, the "7.20" rainstorm was so rare and freakish that the event was seemingly unrelated to the underlying climatology. Finally, the "7.20" rainstorm has led us to realize that such extreme erosive events could and may occur anywhere in eastern China with further implications for soil conservation planning.

## 4 Conclusions

This study evaluated the extreme rainfall events in Henan Province from 20:00 on 16 July 2021 to 20:00 on 22 July 2021, using hourly rainfall data from 797 stations in Henan and surrounding provinces. Based on hourly rainfall data of 2420 meteorological stations in China from 1951 to 2021, the annual maximum daily rainfall erosivity and the annual maximum event rainfall erosivity of Zhengzhou meteorological Station are fitted with the GEV distribution to assess the magnitude and frequency of occurrence of this extreme event. The following conclusions can be drawn as follows:

(1) The maximum event rainfall (785.1 mm), maximum daily rainfall (552.5 mm), maximum hourly rainfall intensity (201.9 $mm \cdot h^{-1}$) and maximum event rainfall erosivity (58,874 $MJ \cdot mm \cdot ha^{-1} \cdot h^{-1}$) of "7·20" rainstorm all occurred at Zhengzhou meteorological station. The period of the highest rainfall intensity was mainly concentrated in the middle and late stages of the storm, reaching its peak on 20 July, producing a daily total of 144.2 $MJ \cdot ha^{-1}$ energy.

(2) Based on observations in the past decades (1951-2020) and the fitted GEV distribution, the "7.20" extreme event was estimated to have an average recurrence interval in excess of 100,000 years, and the annual maximum daily and event rainfall erosivity were about 10 times larger than 1-in-100-year erosivity values.

(3) Zhengzhou meteorological station has set a new record for daily and event rainfall erosivity values in mainland China. The "7.20" rainstorm in 2021 was so rare and freakish, and suggested to us that extreme erosive events could and may occur anywhere in eastern China, rather than in low latitude as we previously knew and expected.

***Data availability.*** Not applicable.

***Author contributions.*** Y Xiao, S Yin and B Yu developed the concepts of the manuscript. Y Xiao conducted calculations and visualization, and wrote the first draft. S Yin and B Yu did methodology, review and editing. C Fan, W Wang and Y Xie did the review and editing.

***Competing interests.*** The authors declare that they have no conflict of interest.

***Disclaimer.*** Publisher's note: Copernicus Publications remains neutral with regard to jurisdictional claims in published maps and institutional affiliations.

***Financial support.*** This research has been supported by the National Key Research and Development Program of China (grant no. 2021YFE0113800), National Natural Science Foundation of China (grant no. 41877068) and the project "ACRP 13: Soil erosion in Austria -from mean to extreme (EROS-A)" funded by the Klima- und Energiefonds.

## References

Alexander, L.V., Hope, P., Collins, D., Trewin, B., Lynch, A., and Nicholls, N.: Trends in Australia's climate means and extremes: a global context, Aust. Meteorol. Mag., 56, 1–18, 2007.

Almagro, A., Oliveira, T. P. S., Nearing, M. A., and Hagemann, S.: Projected climate change impacts in rainfall erosivity over Brazil, Sci. Rep., 7, 8130, https://doi.org/10.1038/s41598-017-08298-y, 2017.

Auerswald, K., Fischer, F. K., Winterrath, T., and Brandhuber, R.: Rain erosivity map for Germany derived from contiguous radar rain data, Hydrol. Earth Syst. Sci., 23, 1819–1832, https://doi.org/10.5194/hess-23-1819-2019, 2019.

Bureau of Hydrology, Changjiang Water Resources Commission, and Nanjing Institute of Hydrology and Water Resources.: Handbook of calculation design flood for water resources and hydropower projects, Hydropower and Electrical Press, Beijing, 2001. (in Chinese)

Borrelli, P., Diodato, N., and Panagos, P.: Rainfall erosivity in Italy: a national scale spatio-temporal assessment, Int. J. Digit. Earth., 9, 835–850. https://doi.org/10.1080/17538947.2016.1148203, 2016.

Bezak, N., Mikoš, M., Borrelli, P., Liakos, L., and Panagos, P.: An in-depth statistical analysis of the rainstorms erosivity in Europe, Catena, 206, 105577, https://doi.org/10.1016/j.catena.2021.105577, 2021.

Bezak, N., Borrelli, P., and Panagos, P.: Exploring the possible role of satellite-based rainfall data in estimating inter- and intra-annual global rainfall, Hydrol. Earth Syst. Sci., 26, 1907-1924, https://doi.org/10.5194/hess-26-1907-2022, 2022

Cao, Y., Wang, S. J., Bai, X. Y., Li, H. W., Wang, M. M., and Wu, L. H.: Inversion calculation and spatial-temporal pattern of rainfall erosivity in southwestern China over one hundred years, Acta Ecol. Sin., 38, 8766–8773, https://doi.org/10.5846/stxb201805241142, 2018. (in Chinese)

Diodato, N., Bellocchi, G., Romano, N., and Guadagno, F. M.: Modelling the rainfall erosivity of the Rhone Region (Southeastern France) associated with climate variability and storminess, Adv. Meteorol., 2016, 7626505, https://doi.org/10.1155/2016/7626505, 2016.

Evans, J.P., Arguesco, D., Olson, R., and Di Luca, A.: Bias-corrected regional climate projections of extreme rainfall in south-east Australia, Theor. Appl. Climatol., 130, 1085–1098, https://doi.org/10.1007/s00704-016-1949-9, 2016.

Fishman, R.: More uneven distributions overturn benefits of higher precipitation for crop yields, Environ. Res. Lett., 11, 024004, https://doi.org/10.1088/1748-9326/11/2/024004, 2016.

Fang, W., Huang, Q., Huang, S. Z., Yang, J., Meng, E. H., and Li, Y. Y.: Optimal sizing of utility-scale photovoltaic power generation complementarily operating with hydropower: a case study of the World's largest hydro-photovoltaic plant, Energy Convers. Manag., 136, 161–172, https://doi.org/10.1016/j.enconman.2017.01.012, 2017.

Fang, W., Huang, S.Z., Huang, Q., Huang, G. H., Meng, E. H., and Luan, J. K.: Reference evapotranspiration forecasting based on local meteorological and global climate information screened by partial mutual information, J. Hydrol., 561, 764–779, https://doi.org/10.1016/j.jhydrol.2018.04.038, 2018.

Gu, Z. J., Feng, D. T., Duan, X. W., Gong, K. F., Li, Y. W., and Yue, T. Y.: Spatial and Temporal Patterns of Rainfall Erosivity in the Tibetan Plateau, Water, 12, 200, https://doi.org/10.3390/w12010200, 2020.

Hosking, J. R. M.: L-Moments: Analysis and Estimation of Distributions Using Linear Combinations of Order Statistics, J. R. Stat, Soc., Ser. B., Methodol., 52, 105–124, http://www.jstor.org/stable/2345653, 1990.

Huang, S. Z., Chang, J. X., Huang, Q., Chen, Y. T., and Leng, G.Y.: Quantifying the relative contribution of climate and human impacts on runoff change based on the Budyko hypothesis and SVM model, Water Resour. Manag., 30, 2377–2390, https://doi.org/10.1007/s11269-016-1286-x, 2016a.

Huang, S., Huang, Q., Chang, J.X., and Leng, G. Y.: Linkages between hydrological drought, climate indices and human activities: a case study in the Columbia River basin, Int. J. Climatol., 36, 280–290, https://doi.org/10.1002/joc.4344, 2016b.

Huang, S., Huang, Q., Leng, G.Y., and Chang, J. X.: A hybrid index for characterizing drought based on a nonparametric kernel estimator, J. Appl. Meteorol. Climatol., 55, 1377–1389, https://doi.org/10.1175/JAMC-D-15-0295.1, 2016c.

Huang, Y. X., Liang, Z. M., Hu, Y. M., Li, B. Q., and Wang, J.: Theoretical derivation for the exceedance probability of corresponding flood volume of the equivalent frequency regional composition method in hydrology, Hydrol. Res., 51, 1274–

https://doi.org/10.5194/hess-2022-351
Preprint. Discussion started: 11 October 2022

Hydrology and Earth System Sciences
Open Access
Discussions

1292, https://doi.org/10.2166/nh.2020.027, 2020.

IPCC.: Climate Change 2021: The Physical Science Basis, Working Group I contribution to the Sixth Assessment Report of the Intergovernmental Panel on Climate Change, Masson-Delmotte, V., P. Zhai, A. Pirani, S.L. Connors, C. Péan, S. Berger, N. Caud, Y. Chen, L. Goldfarb, M.I. Gomis, M. Huang, K. Leitzell, E. Lonnoy, J.B.R. Matthews, T.K. Maycock, T. Waterfield, O. Yelekçi, R. Yu, and B. Zhou (eds.). Cambridge University Press, Cambridge, United Kingdom and New York, NY, USA, In press, https://doi.org/10.1017/9781009157896, 2021.

Jiang, Q., Li, W., Wen, J., Fan, Z., Chen, Y., Scaioni, M., and Wang, J.: Evaluation of satellite-based products for extreme rainfall estimations in the eastern coastal areas of China, J. Integr. Environ. Sci., 16, 191–207, https://doi.org/10.1080/1943815X.2019.1707233, 2019.

Jin, S. Y., Guo, S. M., and H, W. B.: Analysis on the Return Period of "7.20" Rainstorm in the Xiaohua Section of the Yellow River in 2021, Water, 14, 2444, https://doi.org/10.3390/w14152444, 2022.

Klik, A., and Rosner, J.: Long-term experience with conservation tillage practices in Austria: Impacts on soil erosion processes, Soil Tillage Res., 203, 104669, https://doi.org/10.1016/j.still.2020.104669, 2020.

Kilic, O. M. and Gunal, H.: Spatial-temporal changes in rainfall erosivity in Turkey using CMIP5 global climate change scenario, Arabian J. Geosci., 14, 1079, https://doi.org/10.1007/s12517-021-07184-2, 2021.

Klik, A., Haas, K., Dvorackova, A., and Fuller, I. C.: Spatial and temporal distribution of rainfall erosivity in New Zealand, Soil Res., 53, 815–825, https://doi.org/10.1071/SR14363, 2015.

Kebede, S. Y., Endalamaw, T. N., Sinshaw, G. B., and Atinkut, B. H.: Modeling soil erosion using RUSLE and GIS at watershed level in the upper beles, Ethiopia, Environ. Challenges, 2, 100009, https://doi.org/10.1016/j.envc.2020.100009, 2021.

Lu, H. and Yu, B.: Spatial and seasonal distribution of rainfall erosivity in Australia, Soil Res., 40, 887–901, https://doi.org/10.1071/SR01117, 2002.

Liu, B. Y., Zhang, K. L., and Xie, Y.: An empirical soil loss equation. Proceedings-Process of Soil Erosion and Its Environment Effect, 2, 21–25, 2002.

Li, J., Liu, Z. H., and Li, R.: Temporal and spatial characteristics of rainfall erosivity with different geomorphology types on the loess plateau, Bull. Soil Water Conserv., 2, 124–127, https://doi.org/ 10.13961/j.cnki.stbctb.2008.03.025, 2008. (in Chinese)

Li, J., Yu, R. C., and Sun, W.: Duration and Seasonality of Hourly Extreme Rainfall in the Central Eastern China, Acta Meteorol. Sin., 27, 799–807, https://doi.org/10.1007/s13351-013-0604-y, 2013.

Liu, S. L., Huang, S. Z., Xie, Y. Y., Leng, G. Y., Huang, Q., Wang, L., and Xue, Q.: Spatial-temporal changes of rainfall erosivity in the loess plateau, China: Changing patterns, causes and implications, Catena, 166, 279–289, https://doi.org/10.1016/j.catena.2018.04.015, 2018.

Liao, X., Xu, W., Zhang, J., Li, Y., and Tian, Y.: Global exposure to rainstorms and the contribution rates of climate change and population change, Sci. Total Environ., 663, 644–653, https://doi.org/10.1016/j.scitotenv.2019.01.290, 2019.

Michaelsen, J.: Cross-validation in statistical climate forecast models, J. Appl. Meteor., 26, 1589–1600, https://doi.org/10.1175/1520-0450(1987)026<1589:CVISCF>2.0.CO;2, 1987.

Meusburger, K., Steel, A., Panagos, P., Montanarella, L., and Alewell, C.: Spatial and temporal variability of rainfall erosivity factor for Switzerland, Hydrol. Earth Syst. Sci., 16, 167–177, https://doi.org/10.5194/hess-16-167-2012, 2012.

Mello, C. R., Viola, M. R., Beskow, S., and Norton, L. D.: Multivariate models for annual rainfall erosivity in Brazil, Geoderma, 202, 88–102, https://doi.org/10.1016/j.geoderma.2013.03.009, 2013.

Ma, X., He, Y., Xu, J., van Noordwijk, M., and Lu, X.: Spatial and temporal variation in rainfall erosivity in a Himalayan watershed, Catena, 121, 248–259, https://doi.org/10.1016/j.catena.2014.05.017, 2014.

McGehee, R. P., Flanagan, D. C., Srivastava, P., Engel, B. A., Huang, C. H., and Nearing, M. A.: An updated isoerodent map of the conterminous United States, ISWCR, 10, 1–16, https://doi.org/10.1016/j.iswcr.2021.06.004, 2022.

Nearing, M. A., Pruski, F. F., and O'Neal, M. R.: Expected climate change impacts on hillslope erosion rates: a review, J. Soil Water Conserv., 59, 43–50, 2004.

Palharini, R. S. A., Vila, D. A., Rodrigues, D. T., Quispe, D. P., Palharini, R. C., de Siqueira, R. A., and de Sousa Afonso, J. M.: Assessment of the extreme precipitation by satellite estimates over South America, Remote Sens., 12, 2085, https://doi.org/10.3390/rs12132085, 2020.

Panagos, P., Ballabio, C., Borrelli, P., Meusburger, K., Klik, A., Rousseva, S., Tadic, M. P., Michaelides, S., Hrabalikova, M., Olsen, P., Aalto, J., Lakatos, M., Rymszewicz, A., Dumitrescu, A., Begueria, S., and Alewell, C.: Rainfall erosivity in Europe, Sci. Total Environ., 511, 801–814, https://doi.org/10.1016/j.scitotenv.2015.01.008, 2015.

Panagos, P., Borrelli, P., Spinoni, J., Ballabio, C., Meusburger, K., Beguería, S., Klik, A., Michaelides, S., Petan, S., Hrabalikova, M., Olsen, P., Aalto, J., Lakatos, M., Rymszewicz, A., Dumitrescu, A., Tadic, M. P., Diodato, N., Kostalova, J., Rousseva, S., Banasik, K., and Alewell, C.: Monthly rainfall erosivity: Conversion factors for different time resolutions and regional assessments, Water, 8, 119, https://doi.org/10.3390/w8040119, 2016.

Panagos, P., Borrelli, P., Meusburger, K., Yu, B. F., Klik, A., Lim, K. J., Yang, J. E., Ni, J. R., Miao, C. Y., Chattopadhyay, N., Sadeghi, S. H., Hazbavi, Z., Zabihi, M., Larionov, G. A., Krasnov, S. F., Gorobets, A. V., Levi, Y., Erpul, G., Birkel, C., Hoyos, N., Naipal, V., Oliveira, P. T. S., Bonilla, C. A., Meddi, M., Nel, W., Al Dashti, H., Boni, M., Diodato, N., Van Oost, K., Nearing, M., and Ballabio, C.: Global rainfall erosivity assessment based on high-temporal resolution rainfall records. Sci. Rep., 7, 4175, https://doi.org/10.1038/s41598-017-04282-8, 2017.

Petek, M., Mikoš, M., and Bezak, N.: Rainfall erosivity in Slovenia: Sensitivity estimation and trend detection, Environ. Res., 167, 528–535, https://doi.org/10.1016/j.envres.2018.08.020, 2018.

Panagos, P., Borrelli, P., Matthews, F., Liakos, L., Bezak, N., Diodato, N., and Ballabio, C.: Global rainfall erosivity projections for 2050 and 2070, J. Hydrol., 610, 127865, https://doi.org/10.1016/j.jhydrol.2022.127865, 2022.

Qin, W., Guo, Q., Zuo, C., Shan, Z., Ma, L., and Sun, G.: Spatial distribution and temporal trends of rainfall erosivity in mainland China for 1951–2010, Catena, 147, 177–186, https://doi.org/10.1016/j.catena.2016.07.006, 2016.

Renard, K. G., Foster, G. R., Weesies, G. A., McCool, D. K., and Yoder, D. C.: Predicting soil erosion by water: a guide to conservation planning with the revised universal soil loss equation (RUSLE), Agriculture Handbook, US Department of Agriculture, Washington, D. C., 1997.

Sadeghi, S. H. R., Zabihi, M., Vafakhah, M., and Hazbavi, Z.: Spatiotemporal mapping of rainfall erosivity index for different return periods in Iran, Nat. Hazards, 87, 35–56, https://doi.org/10.1007/s11069-017-2752-3, 2017.

USDA-ARS.: Science documentation: Revised universal soil loss equation version2 (RUSLE2), US Department of Agriculture, Agricultural Research Service, Washington, D.C., 2013.

Wang, J. Q.: Rainstorm in China, China Water & Power Press, Beijing, 2002. (in Chinese)

Wischmeier, W. H. and Smith, D. D.: Rainfall energy and its relationship to soil loss, Trans. Am. Geophys. Union, 39, 285–291, https://doi.org/10.1029/TR039i002p00285, 1958.

Wischmeier, W. H. and Smith, D. D.: Predicting rainfall erosion losses from cropland east of the Rocky Mountains, Agriculture Handbook, US Department of Agriculture, Washington, D. C., 1965.

Wischmeier, W. H. and Smith, D. D.: Predicting rainfall erosion losses: A guide to conservation planning, Agriculture Handbook, US Department of Agriculture, Washington, D. C., 1978.

Wang, W. T., Yin, S. Q., Xie, Y., Liu, B. Y., and Liu, Y. N.: Effects of four storm patterns on soil loss from five soils under natural rainfall, Catena, 141, 56–65, https://doi.org/10.1016/j.catena.2016.02.019, 2016.

Wang, W., Yin, S. Q., Gao, G., Papalexiou, S. M., and Wang, Z.: Increasing trends in rainfall erosivity in the Yellow River basin from 1971 to 2020, J. Hydrol., 610, 127851, https://doi.org/10.1016/j.jhydrol.2022.127851, 2022.

Xie, Y., Liu, B. Y., and Zhang, W. B.: Study on standard of erosive rainfall, J. Soil Water Conserv., 14, 6-11,

https://doi.org/10.5194/hess-2022-351
Preprint. Discussion started: 11 October 2022



https://doi.org/10.13870/j.cnki.stbcxb.2000.04.002, 2000. (in Chinese)

Xie, Y., Yin, S. Q., Liu, B., Nearing, M. A., and Zhao, Y.: Models for estimating daily rainfall erosivity in China, J. Hydrol., 535, 547–558, https://doi.org/10.1016/j.jhydrol.2016.02.020, 2016.

Yang, F. and Lu, C.: Spatiotemporal variation and trends in rainfall erosivity in China's dryland region during 1961–2012, Catena, 133, 362–372, https://doi.org/10.1016/j.catena.2015.06.005, 2015.

Yin, S. Q. and Wang, W. T.: A review on the stochastic simulation of rainfall process data for soil erosion assessment, Prog. Geogr., 39, 1747–1757, https://doi.org/1007-6301(2020)39:10<1747:TRQSYJ>2.0.TX;2-4, 2020. (in Chinese)

Yin, S., Xie, Y., Liu, B. and Nearing, M.A.: Rainfall erosivity estimation based on rainfall data collected over a range of temporal resolutions, Hydrol. Earth Syst. Sci., 12, 4965–4996, https://doi.org/10.5194/hessd-12-4965-2015, 2015.

Yin, S. Q., Nearing, M. A., Borrelli, P., and Xue, X. C.: Rainfall Erosivity: An Overview of Methodologies and Applications, Vadose Zone J., 16, https://doi.org/10.2136/vzj2017.06.0131, 2017.

Yin, S., Xue, X., Yue, T., Xie, Y. and Gao, G.: Spatiotemporal distribution and return period of rainfall erosivity in China, Trans. Chinese Soc. Agric. Eng., 35, 105–113, https://doi.org/1002-6819(2019)35:9<105:ZGJYQS>2.0.TX;2-W, 2019. (in Chinese)

Yue, T. Y., Xie, Y., Yin, S. Q., Yu, B. F., Miao, C. Y., and Wang, W. T.: Effect of time resolution of rainfall measurements on the erosivity factor in the USLE in China, ISWCR, 8, 373-382, https://doi.org/10.1016/j.iswcr.2020.06.001, 2020.

Yue, T. Y., Yin, S. Q., Xie, Y., Yu, B. F., and Liu, B. Y.: Rainfall erosivity mapping over mainland China based on high-density hourly rainfall records, Earth Syst. Sci. Data, 14, 665–682, https://doi.org/10.5194/essd-14-665-2022, 2022

Zhou, P. H. and Wang, Z. L.: A study on rainstorm causing soil erosion in the Loess Plateau, J Soil Water Conserv., 6, 1–5, https://doi.org/10.13870/j.cnki.stbcxb.1992.03.001, 1992. (in Chinese)

Zhu, Z. L. and Yu, B. F.: Validation of rainfall erosivity estimators for mainland China, Trans. ASABE, 58, 61–71, https://doi.org/10.13031/trans.58.10451, 2015.

Zhang, Y., Nearing, M. A., Zhang, X. C., Xie, Y., and Wei, H.: Projected rainfall erosivity changes under climate change from multimodel and multiscenario projections in Northeast China, J. Hydrol., 384, 97–106, https://doi.org/10.1016/j.jhydrol.2010.01.013, 2010.

Zhang, X., Yang, H., Wang, X. M., Shen, L., Wang, D., and Li, H.: Analysis on characteristic and abnormality of atmospheric circulations of the July 2021 extreme precipitation in Henan, Trans. Atmos. Sci., 44, 672–687, https://doi.org/10.13878/j.cnki.dqkxxb.20210907001, 2021. (in Chinese)

Zhang, X. K., Feng, L. C., and Cui, X. L.: Study on urban resilient waterlogging control system under 7.20 rainstorm in Zhengzhou — Core area of Fuzhou Binhai New Town, J, Catastrophol., 37, 79-83, https://doi.org/10.3969/j.issn.1000811X.2022.02.014, 2022. (in Chinese)